Water Entry of Projectiles

Tadd T. Truscott,[1] Brenden P. Epps,[2] and Jesse Belden[3]

[1]Department of Mechanical Engineering, Brigham Young University, Provo, Utah 84602; email: truscott@byu.edu

[2]Thayer School of Engineering, Dartmouth College, Hanover, New Hampshire 03755

[3]Naval Undersea Warfare Center, Newport, Rhode Island 02841-1708

Annu. Rev. Fluid Mech. 2014. 46:355–78

The *Annual Review of Fluid Mechanics* is online at fluid.annualreviews.org

This article's doi: 10.1146/annurev-fluid-011212-140753

Keywords

free-surface impact, air entraining, supercavitating, cavity formation, sphere, bullet, ballistics

Abstract

The free-surface impact of solid objects has been investigated for well over a century. This canonical problem is influenced by many physical parameters, including projectile geometry, material properties, fluid properties, and impact parameters. Through advances in high-speed imaging and visualization techniques, discoveries about the underlying physics have improved our understanding of these phenomena. Improvements to analytical and numerical models have led to critical insights into cavity formation, the depth and time of pinch-off, forces, and trajectories for myriad different impact parameters. This topic spans a wide range of regimes, from low-speed entry phenomena dominated by surface tension to high-speed ballistics, for which cavitation is important. This review surveys experimental, theoretical, and numerical studies over this broad range, utilizing canonical images where possible to enhance intuition and insight into the rich phenomena.

1. INTRODUCTION

The sheriff in a Western movie shooting at an outlaw hiding underwater has undoubtedly not considered the physics of projectile water entry. Fortunately for the criminal, unless the bullets are designed to travel underwater (most are not), they will not successfully cause harm. Although projectile water entry has been studied for well over a century, it was not until World War II that the need for better understanding became fully apparent. May & Woodhull (1948) were among the first to systematically study this area. Their early work was based on von Kármán's (1929) investigations regarding seaplane landing floats. Since then, the ideas put forth have found their way into the study of the effects of extreme waves and weather on offshore platforms, the loads imposed on ships during slamming (Faltinsen & Zhao 1997), and even the crashworthiness of aerospace structures (Seddon & Moatamedi 2006), sprayed adhesives, paint aerosols, and ink jet printing.

Perhaps the most important applications related to projectile water entry are in the military. Ship slamming is essentially a periodic water entry problem (Faltinsen & Zhao 1997). Air-to-sea ballistics for antitorpedo defense require stable water entry at shallow angles of incidence (Truscott et al. 2009). Occasionally, water entry is sought to be avoided, as in skipping stones (Clanet et al. 2004), skipping cannonballs (Douglas 1855), and the Wallis bomb (Johnson 1998).

Even some biological creatures utilize similar hydrodynamics to walk on water. For example, the basilisk lizard creates a cavity with each step, pushing on a side of the cavity wall to move forward and pulling its foot out before the cavity collapses (Glasheen & McMahon 1996). Physical insight can also be applied to sports performance research, relating to the water entry of athletes, the drag reduction of swimmers near the free surface, the decrease in cavity formation for divers, and the entry and exit of oars in rowing.

Typical experimental studies of water entry employ high-speed imaging and digital image processing. The earliest images are those of Worthington & Cole (1897), who captured still images using single-spark photography. Modern high-speed cameras can now capture thousands of frames per second at full resolution and upward of one million frames per second at reduced resolution: These cameras are capable of fully capturing the unsteady dynamics of the projectile. Extensive high-speed imaging studies of water entry have been presented (Abelson 1970, Aristoff & Bush 2009, Bell 1924, Bergmann et al. 2009, Duclaux et al. 2007, May 1951, May & Hoover 1963, May & Woodhull 1948, 1950, Richardson 1948, Shi et al. 2000, Thoroddsen et al. 2004, Truscott & Techet 2009b).

1.1. Classification of Water Entry Based on Cavity Formation Mechanism

Broadly speaking, the water entry of projectiles can be categorized by whether a cavity is formed. Cavity-forming cases may be classified by the physical mechanism responsible for cavity creation: air entrainment or supercavitation (see also the sidebar Cavity Formation due to the Leidenfrost Effect).

Air-entraining cavity formation is well represented by the canonical vertical water impact of a sphere, as shown in **Figure 1*a***. The phenomenon is typified by an hourglass-shaped air cavity

CAVITY FORMATION DUE TO THE LEIDENFROST EFFECT

Vakarelski et al. (2011) showed that cavities can also be created by the Leidenfrost effect. A superheated steel sphere forms a robust lubricating layer of water vapor as it passes through a water column. This is a form of low-speed cavitation and is less well studied than the other types of cavity formation in this article.

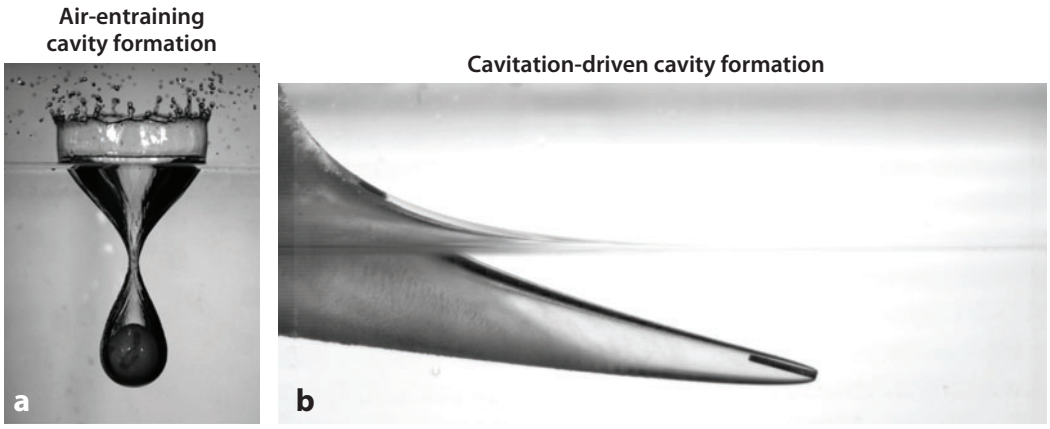

Figure 1

(*a*) Air-entraining cavity formation. A billiard ball falls into a basin of water with sufficient speed to create a subsurface air cavity. Panel *a* reprinted with permission from Truscott & Techet (2009a). Copyright 2009, AIP Publishing LLC. (*b*) Cavitation-driven cavity formation. A bullet enters the water at tremendous speed, causing cavitation as the flow rounds the bullet tip.

extending from the projectile up to the level of the undisturbed free surface and a large splash crown that has been ejected upward. At the air-water-projectile contact line, viscous forces outweigh surface tension forces, and the contact line is pinned to the projectile surface. This allows air to be entrained behind the sphere as the cavity is formed. Although variations in geometry, material properties, and impact conditions add complexity to the air-entraining water entry phenomenon, the global features of the canonical problem shown in **Figure 1*a*** remain prevalent.

In contrast to the relatively low-speed air-entraining case, cavitation is responsible for cavity formation if the projectile speed is large enough. That is, the water actually vaporizes, and the subsurface cavity is filled with an air-steam mixture. When cavitation creates a large-enough vaporous region to encapsulate the projectile, this is known as supercavitation. For example, **Figure 1*b*** shows the relatively high-speed water entry of a bullet.

1.2. Scope and Organization

In this article, we review the two cavity-forming cases (air entraining and supercavitating). We discuss the critical speed required for air-entraining cavity formation, but we do not otherwise discuss the no-cavity case. Readers interested in water entry with no cavity formation are referred to Ern et al. (2012), Horowitz & Williamson (2010), and Truscott et al. (2012a). Additionally, we consider only axisymmetric bodies. We also note that air and water are the fluids of interest, but in theory, the nondimensional results described below apply to any Newtonian fluid (of the same density ratio as air and water).

1.3. Key Parameters

There are several key parameters that affect the physics of the water entry problem. In both the air-entraining and the supercavitating case, the key parameters of the projectile are the geometry (assumed axisymmetric with maximum diameter D), wettability (characterized by the static contact angle θ_0), density ρ_s, and location of the center of mass. The key parameters of the impact event are the impact speed U_0, impact angle α_0, transverse spin Ω_T (spin axis normal to the direction of travel), and longitudinal spin Ω_L (spin axis along the direction of travel). The key parameters of

Capillary number: viscous force divided by the surface tension force; $Ca = \mu U_0/\gamma$

the fluid are the density $\rho = 999$ kg m^{-3}, viscosity $\mu = 1.12\text{E-}3$ kg (ms)$^{-1}$, and surface tension $\gamma = 7.34\text{E-}2$ kg s^{-2}.

From these parameters, a number of important nondimensional parameters can be formed, and we now discuss their typical values. The capillary number $Ca \equiv \mu U_0/\gamma$, wetting angle, and geometry determine whether an air-entraining cavity forms. **Figure 2*c*** shows that the critical

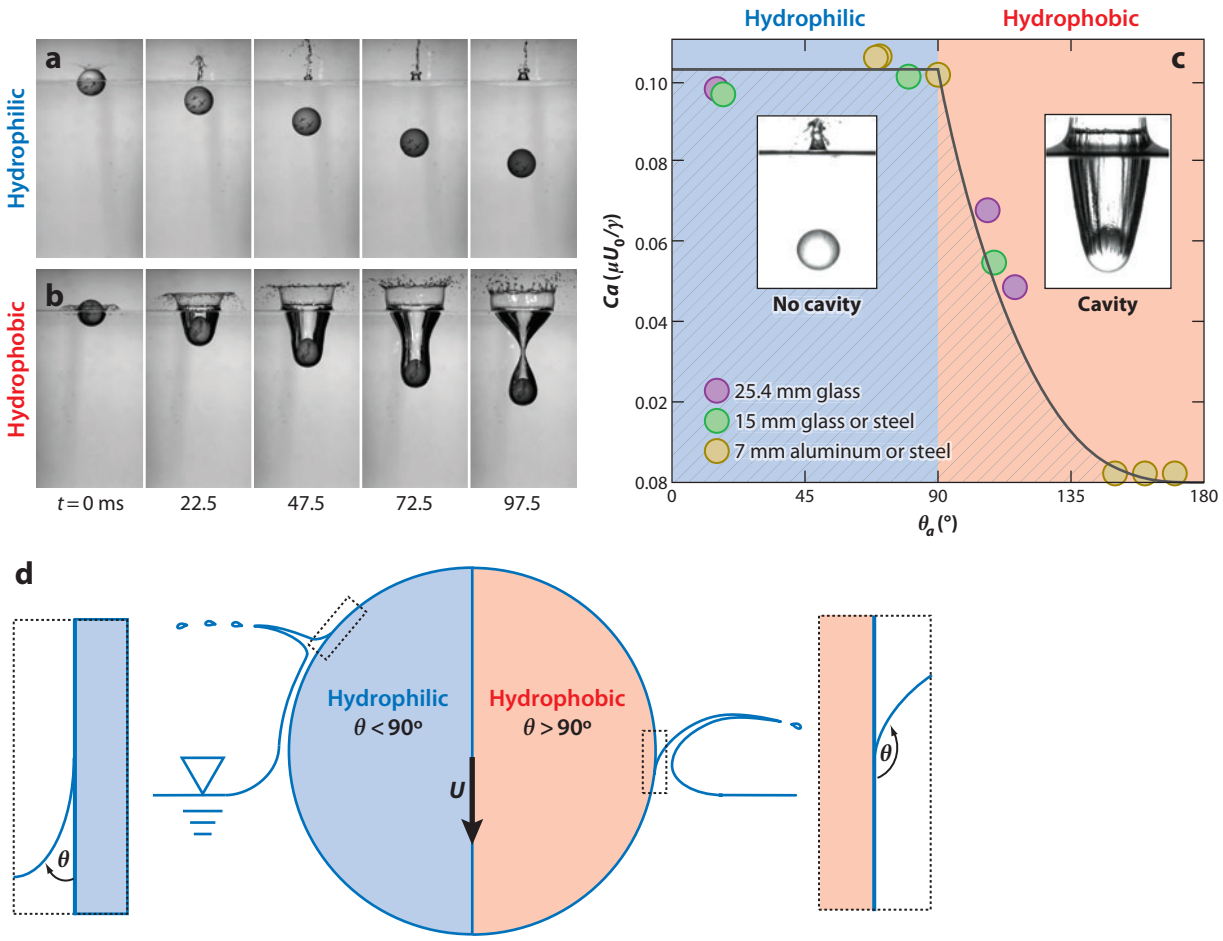

Figure 2

(*a*) The water entry of a hydrophilic billiard ball ($\theta = 67°$) at impact speed $U_0 = 1.72$ ms^{-1}. A large vertical jet is formed in this noncavity-forming case. (*b*) The water entry of a cavity-forming hydrophobic billiard ball ($\theta = 120°$) at $U_0 = 1.72$ ms^{-1}. The sphere is completely encased in a thin layer of air, a large cavity is formed above the sphere, and the splash crown is vertical. Readers are referred to **Supplemental Videos 1–4** for side and top views of the entries shown in panels *a* and *b* (follow the **Supplemental Material link** from the Annual Reviews home page at **http://www.annualreviews.org**). Panels *a* and *b* taken from Truscott & Techet (2009a). Copyright 2009, AIP Publishing LLC. (*c*) Critical capillary number for cavity formation ($Ca = \mu U_0/\gamma$) versus advancing contact angle θ (referred to as θ_a in Duez et al. 2007). A superhydrophobic sphere ($\theta = 180$) will produce a cavity at any impact speed U_0, whereas a hydrophilic sphere $\theta < 90°$ will form a cavity only at larger impact speeds. Interestingly, the critical capillary number (impact speed) is the same for any hydrophilicity $0 \leq \theta < 90°$. Panel *c* taken from Duez et al. (2007), adapted with permission from Macmillan Publishers Ltd.: *Nature Physics*, copyright 2007. (*d*) Illustration depicting how the wetting angle affects water entry behavior. A cavity is formed for the hydrophobic case ($\theta > 90°$, above the critical capillary number), whereas the fluid remains attached for the hydrophilic case ($\theta < 90°$, below the capillary number).

capillary number for the cavity formation of spheres varies with wetting angle and is at most of the order of 0.1. Historically, most studies have been performed at high capillary numbers (i.e., high impact speeds) to ensure cavity formation, but recent studies have investigated water entry near the critical capillary number (e.g., Duez et al. 2007, Truscott et al. 2012a). The Bond number $Bo \equiv \rho g D^2/\gamma$ is the ratio of the gravitational force to the surface tension force; few studies have considered low Bond numbers (exceptions include Aristoff et al. 2008, 2009). The Weber number $We \equiv \rho U_0^2 D/\gamma$ is often used to characterize the cavity breakup and could be used to characterize the splash crown stability: The splash crown is analogous to the canonical water bell or water sheet, which has been studied extensively and is beyond the scope of this review. The Froude number $Fr \equiv U_0/\sqrt{gD}$ characterizes the macroscopic behavior of the cavity: Most studies focus on Froude numbers between 1 and 100. Reynolds number effects are largely ignored in the literature, as most studies are conducted at large Reynolds numbers, $Re \equiv \rho U_0 D/\mu$. Spin is put into nondimensional form as the spin parameter $S \equiv \Omega(D/2)/U_0$. Finally, the mass ratio $m^* \equiv \rho_s/\rho$ has also largely been ignored in the literature because large–mass ratio spheres have minimal deceleration, which greatly simplifies the analytic cavity modeling.

Bond number: gravitational force divided by the surface tension force; $Bo = \rho g D^2/\gamma$

Weber number: inertia force divided by the surface tension force; $We = \rho U_0^2 D/\gamma$

Froude number: inertia force divided by the gravitational force; $Fr = U_0/\sqrt{gD}$

Reynolds number: inertia force divided by the viscous force; $Re = \rho U_0 D/\mu$

Spin parameter: tip speed divided by the forward speed; $S = \Omega(D/2)/U_0$

Mass ratio: projectile density divided by the fluid density; $m^* = \rho_s/\rho$

2. AIR-ENTRAINING PROJECTILES

2.1. Conditions Required for Cavity Formation

Projectile water entry does not necessarily result in the formation of a cavity. **Figure 2*a*,*b*** shows the water entry of two billiard balls at the same impact speed U_0, the only difference being the wetting angle of the sphere surface θ , i.e., hydrophilic ($\theta < 90°$) versus hydrophobic ($\theta > 90°$) as shown in **Figure 2*d***. In these low-speed cases, a cavity forms if the capillary number $Ca \equiv U_0\mu/\gamma$ exceeds a critical value for the given wetting angle (**Figure 2*c***) (Duez et al. 2007, Dussan 1979, Snoeijer & Andreotti 2013). This critical capillary number Ca^* is a piecewise decreasing function of the surface wettability θ (**Figure 2*c***). Whereas the impact speed (and thus the capillary number) of the experiments in **Figure 2*a*,*b*** is the same, the wetting angle for the hydrophobic sphere is sufficiently high to be included in the cavity-forming regime shown in **Figure 2*c*** for the given capillary number.

2.2. Initial Water Impact

The beauty of water entry cavities begins in the first few moments after impact as the fluid is displaced downward and outward, forming a splash curtain and the beginnings of a cavity. A full review of these early stages of water entry is beyond the scope of this article, and they have already been reviewed by Korobkin & Pukhnachov (1988), but we wish to orient the reader to three areas of interest.

First, for impact cases in which the sphere impact velocity is sufficiently high ($Re > 9{,}000$), a small axisymmetric horizontal jet is ejected at great velocity radially outward from the point of contact between the sphere and the liquid surface (Thoroddsen et al. 2004) as shown in **Figure 3**. This jet can reach speeds up to 30 times the impact speed. The initial jet forms in less than 1 ms after impact, is difficult to image, and is distinct from the actual splash crown (also shown in **Figure 3**). Surface tension and compressibility appear to have little effect on the formation (Thoroddsen et al. 2004). Studies of the jet formation for different geometries (i.e., cones, ogives) have not been widely published, but preliminary studies by the authors have shown that the splash crown and initial radial jet are less pronounced in the case of a cone.

Second, relatively little work has been done to quantitatively model or characterize the splash crown until recently. Aristoff & Bush (2009) modeled the splash crown growth and formation

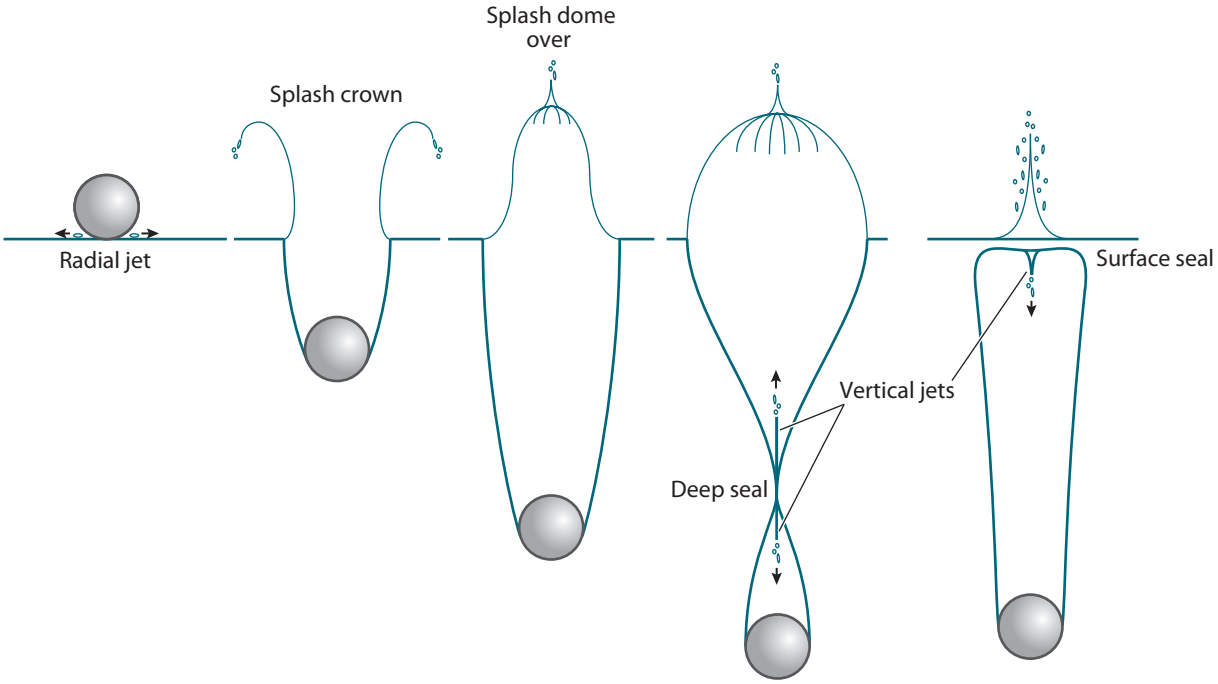

Figure 3

Schematic representing several important features of the water entry event. A radial horizontal jet is formed at the first moment of impact, followed by a larger splash crown. The crown domes over as the sphere descends further into the water column, eventually leading to a deep seal or surface seal as the cavity collapses. These seal events create vertical jets that travel upward and downward from the collapse location.

for moderate–Weber number cases. Their model predicts the splash shape evolution over time relatively well (obviously not accounting for instabilities in sheet thickness or droplet ejection). It also predicts when surface seal occurs with good accuracy.

Third, over very small timescales after impact, the compressibility of the air may be important. If the angle between the body surface and the free surface is small (e.g., a disk impacting normal to its face), then the compressibility of the air layer between the projectile and fluid cushions the impact (Korobkin & Pukhnachov 1988).

2.3. Cavity Classification

As outlined by Aristoff & Bush (2009), there are generally four types of air-entraining cavities that can form after water entry: surface seal, deep seal, shallow seal, and quasi-static seal. A surface seal is characterized by a cavity closure event (called pinch-off) at the free surface with a long cavity attached to the projectile below (see **Figures 3** and **4*a*,*b***). The cavity appears to be pulled under the surface, and then after surface seal multiple pinch-off events occur lower in the water column. A deep seal is characterized by the first pinch-off event occurring much closer to the sphere, typically one-third to one-half of the distance between the sphere and the undisturbed free surface (see **Figure 1*a***). The cavity closure is marked by two distinct jets that form at the singularity where the collapse occurs (**Figure 4*f***). One jet moves up toward the surface, forming the classically named Worthington jet. The formation, shape, and size of these jets have been

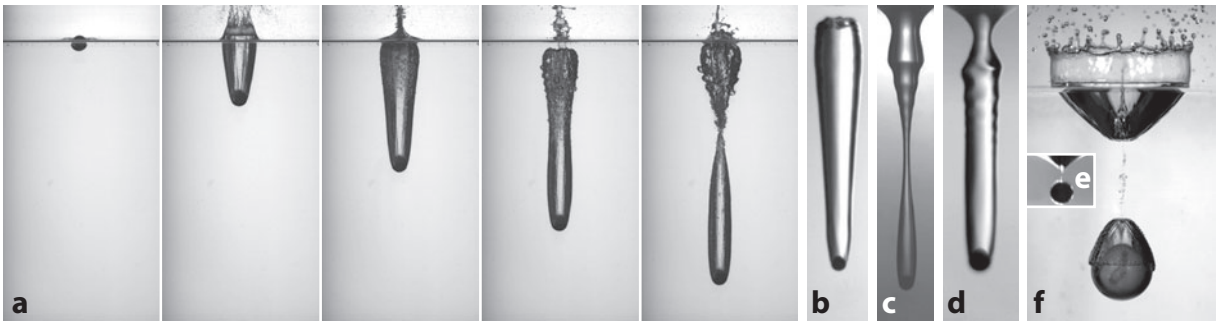

Figure 4

(*a*) The water entry of a 1-inch steel sphere ($Fr = 335$) illustrating surface seal. The time between images is 18 ms. (*b–e*) Images of cavity types: (*b*) surface seal, (*c*) deep seal, (*d*) shallow seal, and (*e*) quasi-static seal. (*f*) Image depicting the two jets that form after collapse. One passes up through the cavity toward the free surface, while the other moves toward the sphere. The image is a subsequent shot from the sequence shown in **Figure 2*b*** and **Supplemental Video 3**. Readers are referred to **Supplemental Videos 5** and **6** for corresponding movies. Panels *b–e* reproduced with permission from Aristoff & Bush (2009).

studied by Antkowiak et al. (2007), Cheny & Walters (1996), Ogawa et al. (2006), and Shin & McMahon (1990). Interestingly, Gekle et al. (2010) found that in the wake of a disk, the air speed in the neck of the collapsing cavity is of the order of the speed of sound in air. When deep seal occurs for slender bodies, pinch off can occur on the body of the projectile, thus altering the jet formation (see **Figures 3** and **5*a***). A shallow seal is characterized by the presence of capillary waves, as seen on the wall of the cavity in **Figure 4*d***. The cavity closure events occur relatively close to the free surface, and the pinch-off appearance is more like a deep seal in which the cavity collapses to a point and the top portion of the cavity forms a large jet. The key difference between a shallow and a deep seal is that pinch-off near the free surface in a shallow seal results from a capillary instability rather than from hydrostatic pressure-driven collapse as for a deep seal (however, observationally they appear very similar) (Aristoff & Bush 2009). A quasi-static seal is characterized by pinch-off at or near the sphere as shown in **Figure 4*e*** ($Ca = 0.0045$, which is well below the critical capillary number for this sphere with $160° < \theta < 170°$); this event occurs for cases in which the sphere is almost unable to enter the water because the surface tension force is nearly large enough to restrain entry. Below we restrict our discussion mainly to the surface and deep seal cases.

For low–Bond number cases, the cavity shape is dependent on the ratio between the surface tension and inertial forces. Aristoff & Bush (2009) presented low–Bond number cases ($10^{-2} < Bo < 10^3$) versus Froude number ($10^{-1/2} < Fr < 10^{5/2}$) with excellent delineations between the four cavity types.

For larger Bond numbers ($Bo > 10^3$), it appears that only surface seal and deep seal occur. Birkhoff & Zarantonello (1957) and Lee et al. (1997) suggested that deep seal occurs roughly halfway between the free surface and the projectile for $\sqrt{20} < Fr < \sqrt{70}$ (using our Froude number definition). The transition from deep seal to surface seal occurs when $Fr > \sqrt{150}$, indicating that the main governing parameters for this event are gravity and inertia. Gilbarg & Anderson (1948) studied how the effects of atmospheric pressure changes would alter cavity closure and cavity behavior. They showed that reduced atmospheric pressures increase the projectile speed required for surface seal. Lee et al. (1997) further argued that for deep seal, the depth of pinch-off is a weak function of the impact velocity, and Froude scaling is likely not useful for anything other than determining the cavity type for high-speed impacts (see the sidebar Cavity Rippling After Closure).

CAVITY RIPPLING AFTER CLOSURE

After cavity closure, a portion of the air cavity typically remains attached to the projectiles. Researchers have noticed a ripple effect in the cavity wake (Grumstrup et al. 2007). It is believed that the formation of these ripples is initiated by the postimpact pinch-off of the cavity. The phenomenon is typical when there is a deep seal followed by a long entrained bubble. The frequency of oscillations increases with increased velocity, and differences in the geometry of the projectiles can alter the ripple shape.

2.4. Cavity Shape

Most studies in recent years have focused on deep seal cases. They often determine the depth and time to pinch-off for varying projectile types. Glasheen & McMahon (1996) proposed a single value of dimensionless pinch-off time, $\tau = t\sqrt{2g/D}$. Data obtained from Truscott & Techet (2009b) yielded $\tau = 1.726 \pm 0.0688$ (mean $\pm$ standard deviation, for 118 trials). This is similar to the value of 1.74 reported by Gilbarg & Anderson (1948) for spheres. Disks also have a constant dimensionless time to pinch-off, but the value is much larger, $\tau = 2.285 \pm 0.0653$ ($n = 47$ trials) (Glasheen & McMahon 1996). Lee et al. (1997) discovered that not only the nondimensional time but also the location of deep closure are nearly constant and independent of the Froude number (impact velocity) for spheres.

Although most studies assume constant velocity, including Lee et al. (1997), Aristoff et al. (2010) revealed that if the mass ratio is reduced, then the deceleration of the spheres with smaller mass ratio can alter the depth of pinch-off, but the nondimensional time to pinch-off—defined in their study as $t^* = tU_0/(D/2)$—remains constant. Images of their findings show this dramatic difference in pinch-off locations but very similar timescales (see **Figure 6**, which shows four different mass ratio spheres entering the water at 2.17 m s^{-1}). If m^* is low enough, the cavity actually collapses on the projectile.

The deep seal cavity shape can also be altered by the geometry of the projectile. **Figure 5** shows cavity shapes produced by several projectile shapes. For slender bodies, the nose shape can affect whether the cavity is large enough to surround the entire projectile before pinch-off or produce a very small cavity. Conical noses produce slender cavities; ogival noses produce larger, more open cavities; and flat noses produce cavities similar to disks doming over the most quickly. Cusped noses (or inverted ogival noses) can produce rather small cavities that wrap up quickly but persist and move along with the tip of the projectile deep into the water (second row in **Figure 5*a***). Altering the radial symmetry can also affect the cavity shape. **Figure 5*b*** shows a 20-pronged disk entering the water, making a beautiful cavity similar to the shape of a pineapple (Enriquez et al. 2012).

2.5. Asymmetric Cavities

Cavity geometry and subsurface trajectory can be made to deviate from the axisymmetric cases presented above, even when the body is geometrically axisymmetric, by altering the angle of a body relative to the surface while maintaining a vertical trajectory prior to impact, imposing an asymmetric wetting angle or introducing transverse spin. **Figure 7** illustrates these effects in the case of an acrylic cylinder ($L/D = 10$) with an ogival nose dropped into quiescent water at 3.1 m s^{-1}. When the body enters the water perpendicular to the free surface, it descends without

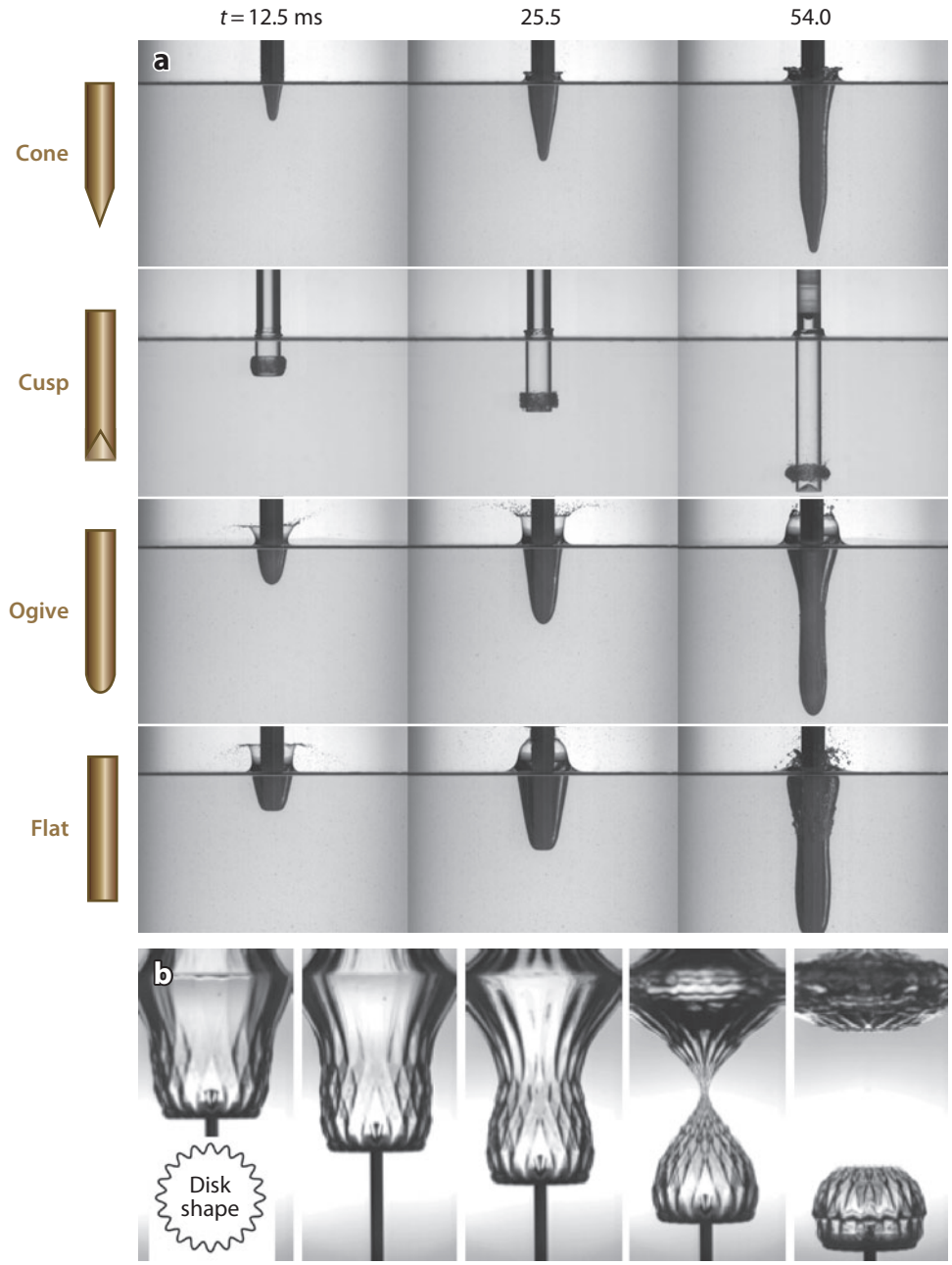

Figure 5

(*a*) The water entry of four different nose shapes (cone, cusp, ogive, and flat) impacting at 3.1 m s^{-1}, illustrating how the nose shape can affect the cavity shape (see **Supplemental Videos 7–10**). Panel *a* taken from Bodily (2013). (*b*) A 20-pronged disk of $d_0 = 20$ mm and $U_0 = 1$ m s^{-1}, creating a pineapple-like cavity, illustrating how an altered radial shape can also affect the cavity shape. Panel *b* reproduced with permission from Enriquez et al. (2012).

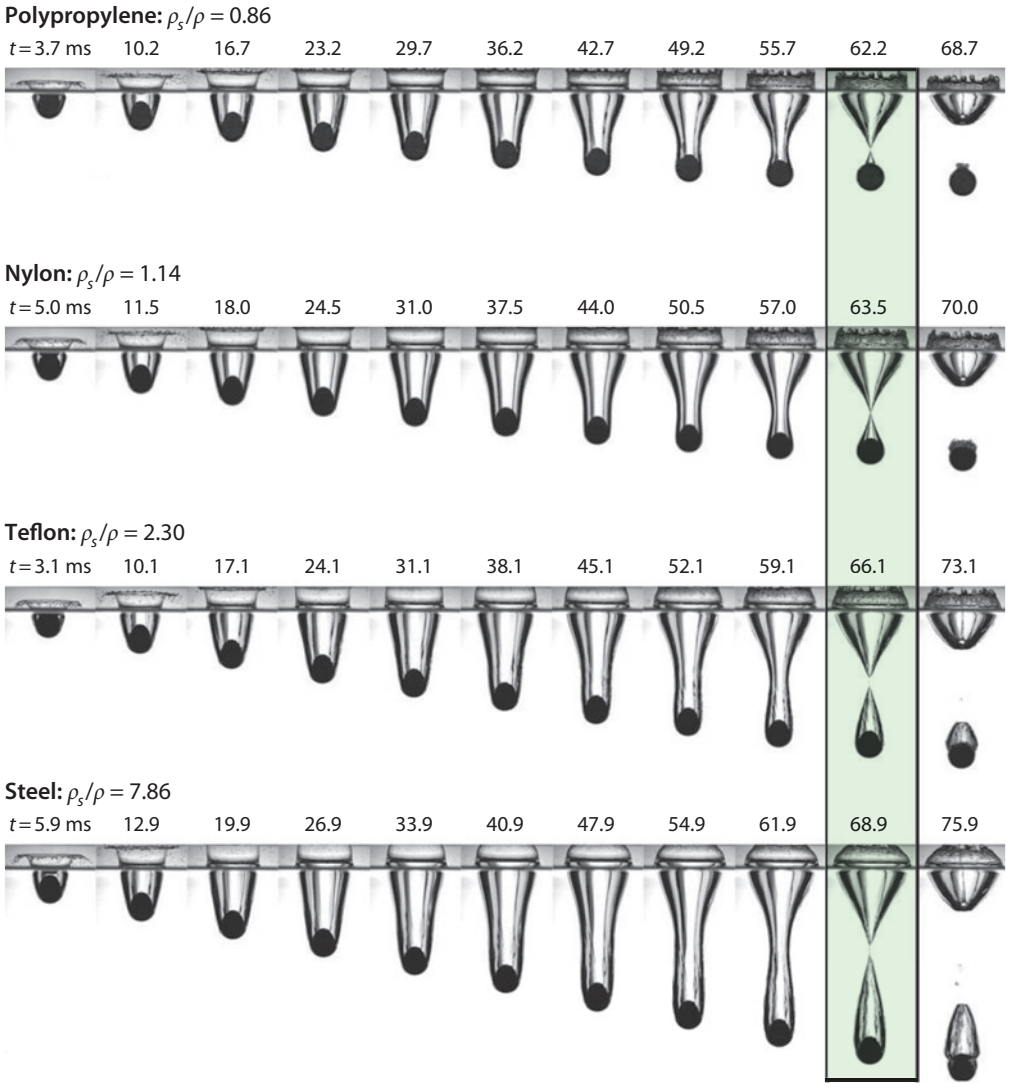

Figure 6

Four different image sequences showing the effects of the mass ratio on the water entry of spheres. Each sphere ($d_0 = 0.0254$ m) impacted the free surface at 2.17 m s^{-1}. The column highlighted in green shows the similarity in the times of pinch-off and the variation of the depth of the sphere and of the depth of the pinch-off event for different mass ratios. Figure reprinted with permission from Aristoff et al. (2010). Copyright 2010, American Institute of Physics.

planar rotation or lateral translation (**Figure 7*a***). Dissimilar wetting angles (**Figure 7*b***; hydrophobic left side $\theta = 141°$, hydrophilic right side $\theta = 63°$) on opposing sides of the body create an asymmetric cavity that turns the nose toward the hydrophilic side. If the cylindrical body impacts oblique to the free surface (**Figure 7*c***; 5° from vertical), a moment couple between the center of pressure and the center of gravity causes planar rotation, thus more dramatically altering the trajectory. Furthermore, a larger impact angle will produce a faster rotation rate and more lateral translation closer to the free surface than a shallow one.

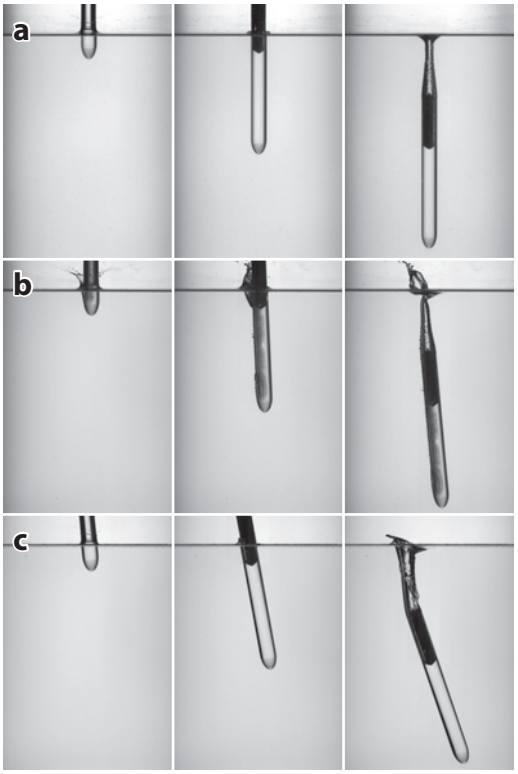

Figure 7

Three acrylic ($\theta = 65°$) slender bodies ($L/D = 10$) entering the water at 3.1 m s^{-1}. The projectiles in panels *a* and *b* are perpendicular to the surface at impact, the projectile in panel *b* is coated with a hydrophobic coating on the left side ($\theta = 141°$), and the projectile in panel *c* is angled normal to the surface by 5°. The time between images is 47.5 ms. Readers are referred to **Supplemental Videos 11–13** for corresponding movies. Figure taken from Bodily (2013).

Spinning a projectile in the transverse direction can induce lift and can alter the trajectory and cavity shape similar to an oblique entry. In fact, if the spin is great enough, a sphere can actually eject from the water surface following a period of underwater travel (Dupeux et al. 2010). Truscott & Techet (2009b) showed that for spheres, the spin modified the trajectory much like the angled cases of **Figure 7**. Their work revealed that the depth of and time to pinch-off are unaffected by the spin rate but that the cavity shape is greatly altered, with the cavity becoming nonaxisymmetric and taking on the shape of a cardioid (**Figure 8*a***). In follow-on studies, they showed that a similar effect could be produced by simply coating half the sphere in a hydrophobic coating (**Figure 8*b***) (Techet & Truscott 2011, Truscott & Techet 2009a).

2.6. Oblique Entry of Low-Speed Projectiles

When the velocity vector of the projectile is no longer normal to the surface, the dynamics of the problem may be dramatically altered. For some combinations of entry angle and the other impact parameters, the projectile may actually ricochet or skip off the surface. Ricochet may be thought of as a special case of water entry in which the vertical direction of velocity is reversed,

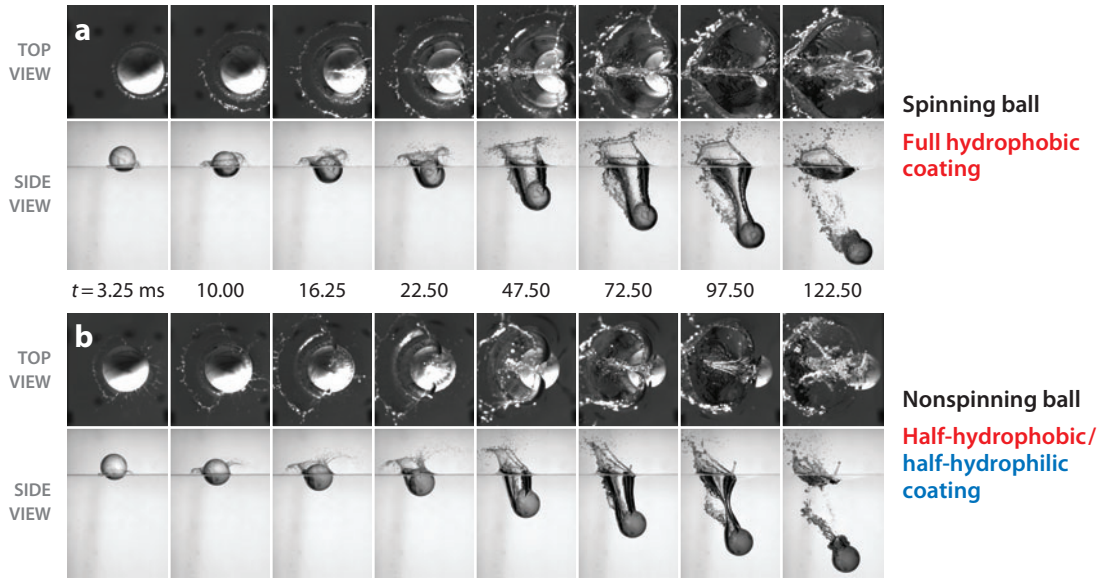

Figure 8

(*a*) Top and side views of a spinning billiard ball with hydrophobic coating ($\theta = 120°$, $U_0 = 1.72$ m s^{-1}, $\Omega_T = 218$ rad s^{-1}, and $D = 5.715$ cm). Viewed from above, the sphere creates a cardioid-shaped splash curtain and subsurface air cavity as it descends in the fluid. On the left side of the sphere, the dynamic wetting angle is large because of an advancing contact line, thus forming a large outward splash. On the right side, the relative velocity is upward because the spin parameter is greater than 1 [$S = \Omega_T (D/2)/U_0 = 3.62$], creating a receding contact line that inhibits splash growth and helps to draw a wedge of fluid across the cavity. (*b*) Top and side views of a nonspinning billiard ball with a half-hydrophobic and half-hydrophilic surface treatment ($\theta_{\text{left}} = 120°$, $\theta_{\text{right}} = 68°$, $U_0 = 120$ m s^{-1}, and $\Omega_T = 0$ rad s^{-1}). The hydrophobic surface coating results in a cavity on the left-hand side, whereas on the right-hand side, the hydrophilic surface inhibits cavity formation, allowing fluid to be driven up around the sphere. Amazingly, a cardioid-shaped cavity is observed similar to the spinning case. In both panels, the first four images are spaced by $t = 6.25$ ms, and the next four are spaced by 25 ms. Readers are referred to **Supplemental Videos 14–17** for corresponding movies. Figure taken from Truscott (2009).

causing the projectile to lift off the surface. Ricochet may be unwanted (in the case of bullet or missile water entry) or may actually be the desired outcome. Eighteenth-century naval tacticians recognized the utility of skipping cannonballs along the water surface to enhance range and accuracy (Douglas 1855). English scientist Sir Barnes Wallis invented a bouncing bomb designed to breach German dams and used during World War II. These bouncing bombs were cylindrical and were launched from aircraft with high velocity and backspin and impacted the water at shallow angles. They skipped along the surface until striking the desired target (for a review, see Johnson 1998). Motivated by these applications, Johnson & Reid (1975) reviewed the ricochet of spheres off water and highlighted the empirical observation that ricochet does not occur if the entry angle exceeds the critical angle given by $\theta_c = 18°/\sqrt{\rho_s/\rho}$, where ρ_s is the density of the sphere. This critical angle was observed to increase only slightly with increasing Froude number. In a more playful setting, Clanet et al. (2004) and Rosellini et al. (2005) investigated the physics of skipping stones and determined that the optimal attack angle for a gyroscopically stabilized stone is 20°. Recently, Truscott et al. (2012b) and Belden et al. (2013) investigated the oblique water impact of highly compliant elastomeric spheres. **Figure 9** shows three impacts of the same elastomeric sphere with the same launch angle but different velocities. In the top sequence, the sphere deforms rapidly into a disk-like shape on impact, thus increasing the wetted area and

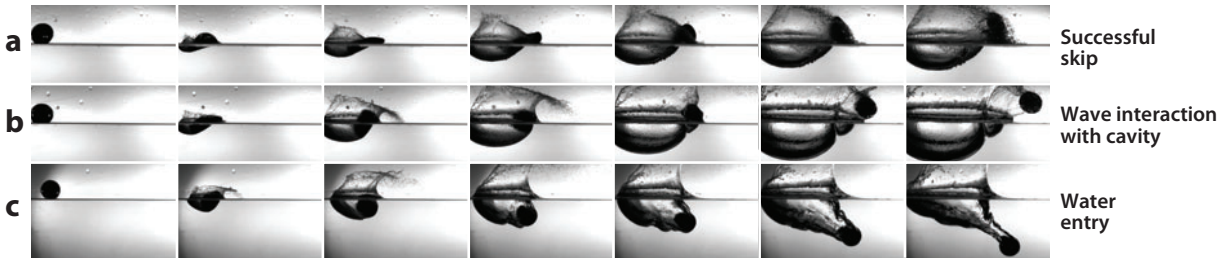

Figure 9

Three impacts of the same elastomeric sphere with the same launch angle but different velocities, showing a successful skip (*a*), a material wave interacting with the cavity (*b*), and a water entry (*c*) (see **Supplemental Videos 18–20**).

force coefficient, causing the sphere to more readily lift off the surface. The middle sequence highlights an interesting phenomenon in which a material wave is initiated on the sphere on impact. This wave then propagates around the sphere periphery and impacts the initial cavity before the sphere leaves the surface. These material deformations are responsible for the wavy disturbances on the cavity for the water entry case shown in the bottom sequence in the figure. Successful skipping was observed for these elastomeric spheres at critical angles of nearly twice that predicted by the empirical relation reported by Johnson & Reid (1975) ($\theta_c = 18°/\sqrt{\rho_s/\rho}$).

2.7. Modeling the Cavity and Projectile Dynamics

The typical assumptions made when modeling cavity-forming water entry of spheres are as follows: inviscid flow (as typically $Re > 10^4$), incompressible flow (as typically $U_0 \ll 1{,}481$ ms^{-1}, the speed of sound in water), and uniform atmospheric pressure for the air above the water surface (as$\rho_{air}/\rho_{water} \ll 1$). Moreover, because the Bond number is typically large, one can also ignore the surface tension force (acting on the body at the contact line). It is worth pointing out Truscott et al. (2012a) showed that for non-cavity-forming water entry of spheres, significant vorticity is shed into the wake and contributes to larger drag forces than for the cavity-forming cases. The ensuing discussion focuses on cavity-forming cases for which no vortices are shed into the sphere wake.

For a free-falling projectile, a simple free-body diagram yields the equation of motion:

$$m\frac{dU}{dt} = mg - F(t). \tag{1}$$

Here $U(t)$ is the instantaneous projectile speed (in the downward direction), m is the projectile mass, g is the gravitational acceleration (downward), and $F(t)$ is the instantaneous hydrodynamic force acting on the projectile (defined as positive upward):

$$F(t) = \int_{BS} p(-\hat{\mathbf{n}} \cdot \hat{\mathbf{k}}) dS, \tag{2}$$

where $\hat{\mathbf{n}}$ is the unit vector pointing out of the body, and $\hat{\mathbf{k}}$ is the unit vector in the z direction (positive upward). The static pressure p is assumed zero (gauge pressure) in the cavity as discussed above. On the wetted body surface, the pressure is given by the unsteady Bernoulli equation,

$$\rho\frac{\partial\phi}{\partial t} + \frac{1}{2}\rho|\nabla\phi|^2 + \rho g z + p = 0, \tag{3}$$

where the velocity potential ϕ varies both spatially and temporally.

Epps (2010) verified that Equations 1–3 accurately represent the dynamics of a sphere falling vertically into the water. Using experimentally measured sphere position and cavity shape data, he implemented a boundary element method to determine ϕ for the observed impact event. He then verified that the hydrodynamic force on the projectile calculated from Equation 2 agreed well with the hydrodynamic force on the projectile inferred from the experimentally derived acceleration and thus the force from Equation 1.

Of course, to develop a fully predictive dynamic solver, one would need to determine the velocity potential ϕ by solving Laplace's equation with the appropriate boundary conditions: quiescent fluid far from the body, no flow through the body surface, the standard free-surface kinematic and dynamic conditions, and the initial condition of $\phi = 0$ on the undisturbed free surface just before impact. For the vertical entry of axisymmetric bodies, Laplace's equation can be solved in a meridional plane, which greatly simplifies the analysis. Any numerical implementation of this model will do the following at each time step: solve Laplace's equation, determine the fluid pressure field from the current and past values of ϕ using Equation 3, integrate the fluid pressure over the body to get the force using Equation 2, determine the acceleration of the body using Equation 1, and update the position of the projectile and free surface. This approach and similar potential flow solvers have been implemented numerically by several authors (Abelson 1971, Bergmann et al. 2009, Birkhoff & Isaacs 1951, Gaudet 1998, Longuet-Higgins & Cokelet 1976, Miloh & Shukron 1991, Yan et al. 2009, Zhao & Faltinsen 1993). Analytical approaches based on this model have been made as well (e.g., Aristoff & Bush 2009, Duclaux et al. 2007, Lee et al. 1997).

One of two simplifying assumptions is often made in the recent literature. The first is that of constant speed $U(t) = U_0$, which is valid only in the case of high–mass ratio projectiles (e.g., steel and tungsten). Alternatively, those that do account for deceleration often assume that the force on the sphere can be modeled as $F(t) = \frac{1}{2}\rho\,[U(t)]^2\,C_D(\pi D^2/4)$ with a prechosen, constant drag coefficient C_D (e.g., Aristoff et al. 2010). However, Truscott et al. (2012a) showed that for low–mass ratio spheres, not only is the projectile decelerating, but also the force coefficient is unsteady.

In any model, careful attention must be paid in the treatment of the contact line dynamics; in particular, the location and angle at which the fluid separates from the projectile greatly affect the resulting cavity shape. Most authors pin the cavity to an experimentally observed point on the projectile surface (e.g., the equator of a sphere) and set the flow separation angle based on observations as well. To achieve a fully predictive numerical model of water entry for an arbitrary body and surface wettability, one must model the contact line dynamics. To our knowledge, this remains an open research issue.

2.8. Modeling the Dynamics in the First Few Moments of Impact

Much work has also been done to model the impact forces during the initial stages of water impact, before the body has submerged more than one-half the diameter. This body of work is distinctly different than the modeling efforts described above, as restricting the analysis to the first few moments of impact allows one to make additional simplifying assumptions. In the work of von Kármán (1929) and many theoretical investigations since, the quadratic pressure term has been neglected and the unsteady term written in terms of an added mass coefficient. The vertical force is then given as $F_3 = d(A_{33}V)/dt$, where A_{33} is the added mass coefficient in heave; keeping A_{33} inside the derivative accounts for the dependence of the amount of the body in contact with the fluid on the submergence (and thus time). A major contribution put forth in Wagner's (1932) theory accounted for the fluid surface in contact with the body rising with

respect to the undisturbed free surface; this has been shown to have a significant effect on the resultant force. More advanced mathematical theories and a history of the problem in the years since have already been reviewed by Korobkin & Pukhnachov (1988); notable contributions have been made by Dobrovolskaya (1969), Miloh (1991), and Faltinsen & Zhao (1997). More recently, Korobkin & Scolan (2006) presented a linearized Wagner approach for several three-dimensional shapes. Faltinsen & Zhao (1997) compared several theoretical and numerical models of sphere water impact and showed that theories that neglect the quadratic pressure term tend to be valid for dimensionless submergence depths up to $U_0 t/D \approx 0.2$. The inclusion of the quadratic pressure term in numerical methods led to more accurate force predictions. These results were supported by the experiments of Moghisi & Squire (1981) in which a force gauge, which was directly attached to a sphere, was used to measure the forces on the sphere during water impact for Reynolds numbers less than 10^4. Laverty (2004) analyzed the forces on a sphere between initial impact and the time corresponding to a submergence of one-fourth the diameter from high-speed digital video data (1,500 frames per second) and found good agreement with the generalized Wagner formulation developed by Miloh & Shukron (1991) for Reynolds numbers between 2^5 and 10^5. Thus, the rate of change of momentum of the added fluid mass is the dominant contributor to the vertical force in the initial stages of impact, with the quadratic pressure term becoming important even at small values of body submergence.

3. SUPERCAVITATING PROJECTILES

3.1. Conditions Required for Supercavitation

Projectiles traveling at high velocities in water can cause the water to cavitate (i.e., vaporize local pockets of the liquid) (Knapp et al. 1970). Cavitation can occur in a flow field when the static pressure is less than the vapor pressure. The susceptibility for cavitation is governed by the cavitation number $\sigma = (p_\infty - p_v)/(0.5\rho U^2)$, where p_∞ is the local hydrostatic pressure, p_v is the vapor pressure of the fluid, ρ is the fluid density, and U is the projectile speed (May 1975). Because cavitation depends on the local pressure in the flow field, which is in turn determined by body shape and motion at entry, there is no single empirical value for σ below which cavitation is guaranteed and above which it is not possible. Generally speaking, very high impact speeds yield low cavitation numbers (high susceptibility), and geometries involving sharp edges such as the bullet shown in **Figure 10*a*** are particularly susceptible.

Savchenko (2001) categorized three stages of cavitation as related to projectile motion: (*a*) initial cavitation, characterized by the formation of small vaporous bubbles; (*b*) partial cavitation, a transient stage of unstable bubble growth; and (*c*) supercavitation, in which a fully

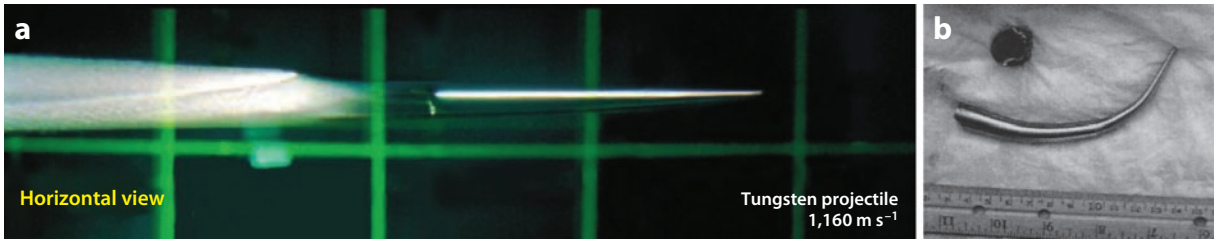

Figure 10

(*a*) Underwater photograph of a high-speed supercavitating bullet. (*b*) Projectile bent during supercavitating water entry. Figure taken from Hrubes (2001, figure 7) with kind permission from Springer Science + Business Media.

developed cavity encapsulates the projectile. Rood (1991) reviewed early developments in the understanding of cavitation inception, and the underlying physics of cavitation bubble growth/collapse was reviewed by Plesset & Prosperetti (1977). The supercavitating regime is still an intensely studied area, particularly as a potential means of drag reduction (Ashley 2001). A supercavity tends to be very elongated owing to the slender geometry and high speed of the projectiles. Because only a small portion of the projectile actually contacts the liquid, the viscous drag on the projectile is dramatically reduced when riding inside a supercavity. Despite this interesting phenomenon, relatively few studies of traveling supercavitating bodies have been published. Recently, Weiland & Vlachos (2012) investigated the inception and growth of cavitation over cylindrical projectiles entering normal to the water surface at high speed. In one of the first and best studies of its kind, Hrubes (2001) investigated bullet water entry at speeds faster than the speed of sound in water (1,481 m s^{-1}). **Figure 10*a*** shows a supercavitating projectile from this study. A large body of literature has also been dedicated to the study of artificial (also known as ventilated) supercavities (Franc & Michel 2004), but we limit our review to naturally formed cavities.

3.2. Modeling the Supercavitation Case

Several theoretical cavity models have been developed. Logvinovich (1972) and Paryshev (2006) developed analytical models for cavity formation and cavity oscillations based partially on empirical data and mostly on control volume analysis. Others have focused more on projectile stability (e.g., Savchenko et al. 2000). Hassan (1999) modeled the planing forces on a supercavitating projectile. Grady (1979) wrote an entire volume of work on the subject of hydroballistics, which includes a excellent summary of both quantitative and qualitative experimental data taken by May (1952, 1975; May & Hoover 1963). More recently, Neaves & Edwards (2006) used a numerical simulation employing preconditioning to estimate the cavity shape, temperature, shock formation, and pressure inside and outside the cavity of projectile water entry.

3.3. Water Entry of High-Speed Projectiles

An extension of the research presented in Section 2.6 is the high-speed, oblique water entry of projectiles such as military ballistics. Projectiles that impact the water at shallow angles are more prone to ricochet. If they do pierce the surface, they often break up or tumble owing to instabilities (see **Figure 11**). An understanding of the oblique water entry of high-speed ballistics is important for improving defensive weapon technology, yet the published research is scarce. Several experimental studies have looked at the vertical air-water impact of high-speed projectiles (e.g., Gilbarg & Anderson 1948, May 1952, Shi et al. 2000, Weiland & Vlachos 2012). Full-scale, shallow-angle, air-to-water studies have been performed by different research groups at several laboratories around the world, but none has been formally published to date.

Unpublished results from tests performed by a group at the Naval Undersea Warfare Center (NUWC) in Newport, Rhode Island, revealed that projectiles with flat noses, tapered tips, and high length-to-diameter ratios (*L/D*) can pierce the surface at shallow angles and continue to descend through the water column without ricochet (Gomez & Shukla 2001, Hrubes 2001) (see **Figure 10**). The experiments revealed that these types of projectiles are stabilized underwater through the hydrodynamic planing of the rear portion of the projectile against the cavity side walls (Hrubes 2001). Stability was observed to be highly sensitive to the bullet and cavity geometry, with catastrophic destabilization leading to a tungsten bullet bending beyond its yield strength (see **Figure 10*b***).

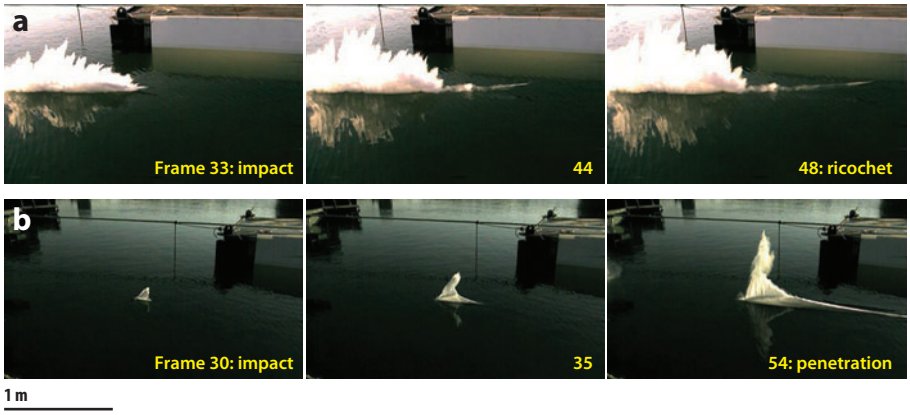

Figure 11

Series of high-speed images showing the water entry of two different projectiles. The time between images is unknown. (*a*) A 0.50-caliber bullet (length ~8 inches, $U_0 \sim 975$ m s^{-1}, and impact angle $= 3.0°$) ricochets off the water surface. (*b*) A different 0.50-caliber bullet (length ~8 inches, $U_0 \sim 975$ m s^{-1}, and impact angle $= 2.8°$) successfully penetrates the surface. Raw images courtesy of J. Gomez & J. Miranda (NUWC).

3.4. Projectile Stability

Because of the high speeds, shallow entry angles, and projectile geometry, the water entry of bullets is more prone to projectile instability than the low-speed cases reviewed in Section 2. This presents a challenging problem for air-to-water ballistics applications, as the projectile must be stable in both air and water. The parameters that the designer can tune are the *L/D*, material (to achieve a desired bending stiffness), exterior geometry, and spin rate. The conundrum is that the design drivers for stability in air oppose the design drivers for stability in the supercavity: Stability in air favors a small *L/D* and a high spin rate about the longitudinal axis (which provides gyroscopic stabilization), whereas stability in a supercavity favors a large *L/D*.

Projectiles are notoriously unstable underwater (e.g., **Figure 12*a*** shows a 0.22-caliber bullet tumbling in its cavity). In fact, supercavitating projectiles are inherently unstable, as the hydrodynamic force acting on the tip almost always causes a pitching moment (similar to balancing a baseball bat vertically on one's hand). The pitching moment rotates the back end of the projectile into contact with the wall of the supercavity, creating a small hydroplaning surface (which in turn produces a righting moment that pushes the projectile back into the cavity). Projectiles with a large *L/D* have a longer moment arm for this righting moment and have a reduced pitch angle between cavity contact resulting in a higher rebound frequency and improved stability.

The larger the *L/D*, the larger is the longitudinal spin rate needed to achieve gyroscopic stability in air. The crux of the problem is that for the desired *L/D* for hydrodynamic stability, the spin rate required for aerodynamic stability may be unfeasibly large. In an unpublished study, a group from NUWC tested the air–to–water entry performance of projectiles with various spin speeds and geometries. They found that nonspinning projectiles were just as unstable underwater as the projectiles spinning at traditional speeds, suggesting that perhaps larger spin rates are required than those expected for traditional aerodynamic flight. They observed that spin rates sufficiently large to stabilize the projectiles actually excited the first natural mode of vibration, thus causing the projectiles to deform. Truscott et al. (2009) successfully demonstrated stable air-to-water flight for spinning projectiles with relatively small *L/D*; the design of these bullets is presented as a case study in Section 3.5.

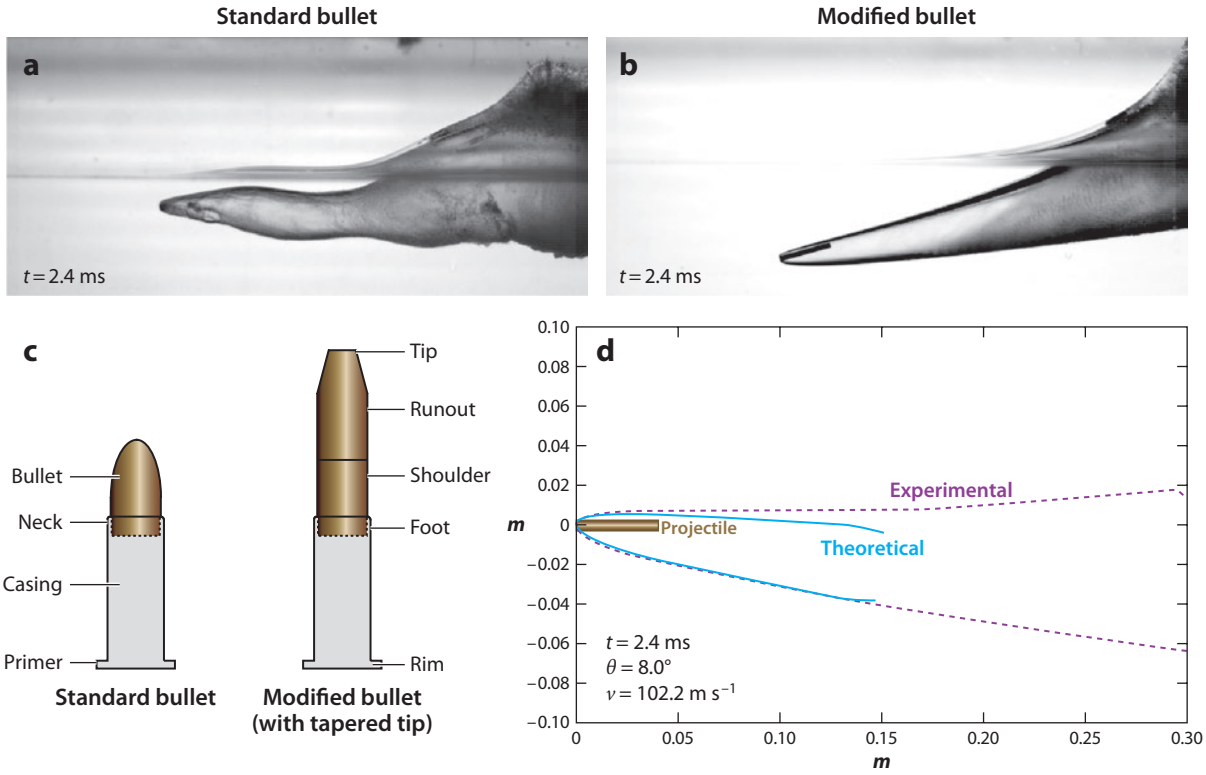

Figure 12

(*a*) A standard 0.22-caliber aluminum bullet tumbling within its cavity, leading to an erratic trajectory and low penetration depth. (*b*) A modified 0.22-caliber aluminum bullet tracking straight, with stability provided by the cavity wall. (*c*) The standard 0.22-caliber bullet design and a modified tapered tip design (not to scale) used in **Figure 13**. (*d*) Comparison of the theoretical cavity shape (*black*) predicted by the modified Logvinovich model (which was used to design the bullet in panel *b*) with the experimentally measured cavity shape (*purple*). The experimental data are rotated into bullet-aligned coordinates with the bullet as shown. For movies corresponding to the water entry shown in panels *a* and *b*, readers are referred to **Supplemental Videos 21** and **22**, respectively. **Supplemental Videos 23** and **24** highlight in color the water entry of a modified 0.22-caliber bullet and a standard 0.22-caliber bullet, respectively. Panels *a–c* taken from Truscott et al. (2009) and panel *d* taken from Truscott (2009).

Longer aerodynamic projectiles tend to be stabilized using fins or body flare at the aft end. Fins and flaring counteract the overturning moment by moving the aerodynamic center of pressure behind the center of gravity, thus making the projectile inherently stable in air. Experiments using fin-stabilized projectiles aimed at shallow angles to the water surface have flown in air stably; however, once underwater, finned projectiles do not travel in a straight path and tend to break into pieces because their fins often come in contact with the cavity side walls (Kocheadorfer 1993). Certainly, open basic and applied research avenues still exist related to the stable air-to-water flight of supercavitating projectiles.

3.5. Design of Water-Surface-Piercing Ballistics

Design is the heart of engineering and requires the synthesis of fundamental and applied scientific research for engineering decisions. In the design of surface-piercing projectiles, such decisions

include the geometry, speed, and angle of impact. Most bullets break up or ricochet because they are designed for air not water (**Figure 12*a***). For axisymmetric (cylindrical) bullets, the geometry is fully defined by the diameter as a function of distance from the tip to tail, $D(x)$. A typical supercavitating projectile will have a flat tip with nonzero diameter $D(0) > 0$. The design of the geometry [i.e., determining $D(x)$] can be carried out using the theory of Logvinovich (1972) and Hassan (1999), which was improved by Truscott (2009). They determined the desired speed, spin rate, angle of incidence, and tip diameter for straight and level flight of a bullet traveling underwater. The resulting cavity shape is illustrated in **Figure 12*d***. The bullet diameter $D(x)$ is then determined to fit within the package space afforded by the cavity. The bullet shown

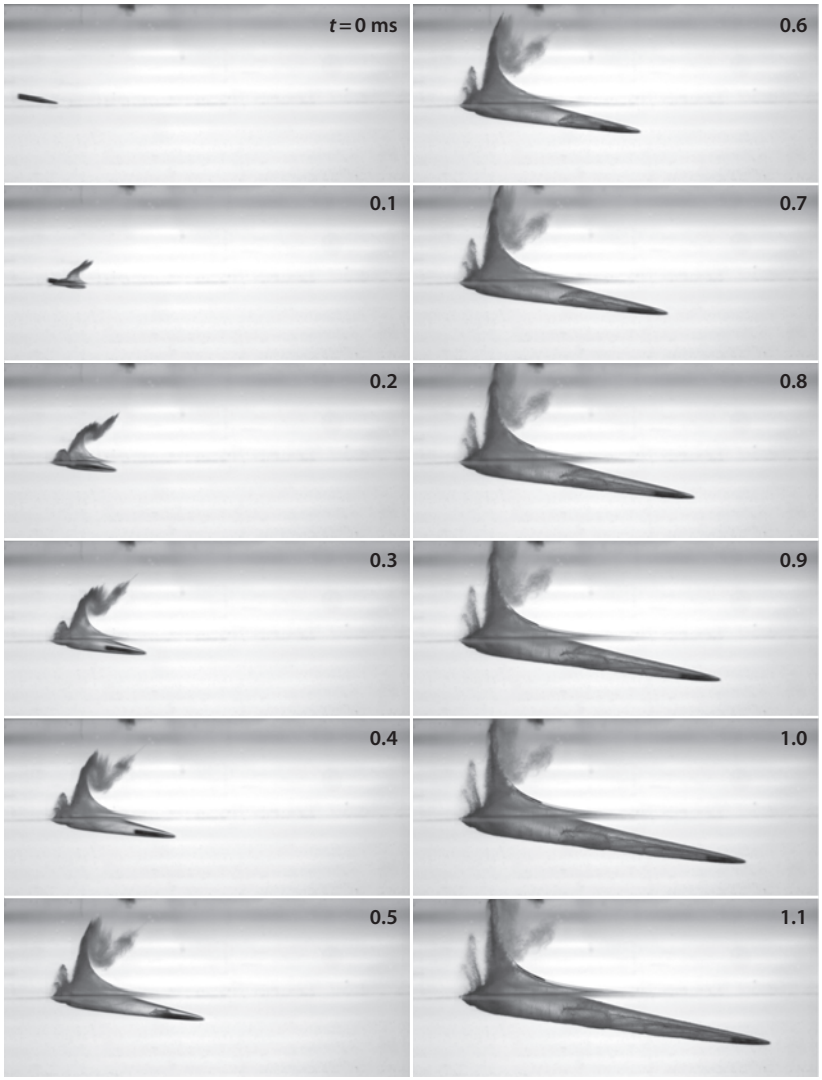

Figure 13

Time series of a modified 0.22-caliber aluminum bullet (with a tapered tip) showing successful water entry and streamlined cavity shape (see **Supplemental Video 25**). Figure taken from Truscott (2009).

in **Figure 12*d*** is a simple cylinder, which fits within the cavity. The total runout (i.e., length between the shoulder and chamber, as shown in **Figure 12*c***) of the bullet is chosen to achieve the desired projectile mass (e.g., 40 grains) and refitted into the projectile housing (**Figure 12*c***). Experimental data proved that this design process works, as seen in the relatively straight flight of **Figure 12*b*** and the good agreement between the experimental cavity and theoretical one in **Figure 12*d***. When properly designed using a combination of modeling and empirical information, supercavitating projectiles can create cavities just the right size and travel long distances underwater. **Figure 13** shows the water entry and downstream run of a modified 0.22-caliber bullet with a smaller tapered nose than that of **Figure 12*d***. Stabilization through contact with the inside of the cavity wall is apparent at $t = 0.5$ ms (Truscott 2009, Truscott et al. 2009).

SUMMARY POINTS

1. Two physical processes are responsible for cavity formation: the deformation of the free surface in the low-speed air-entraining cases and cavitation in the high-speed supercavitating cases.
2. Air-entraining cavity formation occurs when the capillary number exceeds a critical value, which is a function of the wettability of the surface.
3. Asymmetric cavity shapes can be created by geometric asymmetry, transverse spin, or manipulation of the surface wettability.
4. Because typical water entry problems occur at very high Reynolds numbers, both the cavity dynamics and projectile dynamics can be successfully modeled using potential flow theory.
5. Cavitation susceptibility depends on body geometry and the cavitation number.
6. Supercavitating bullets (with large L/D) are often stabilized in air by fins or flaring but not by spin. In water, they are stabilized by leaning against the cavity wall.
7. Research regarding supercavitating cavity dynamics has informed the design of high-speed surface-piercing ballistics.

FUTURE ISSUES

1. The modeling of the contact line dynamics in the air-entraining case should be improved through the synthesis of the macroscopic results presented above with the microscopic results of Snoeijer & Andreotti (2013). This will enable a fully predictive dynamic model of air-entraining projectile water entry for arbitrary body geometry and impact velocity.
2. Experimental and theoretical work needs to be performed to investigate the dynamics of the surface seal cavity case (e.g., cavity shape, trajectory, and forces versus Fr, Re, and m^*).
3. The influence of cavitation should be determined: How does the introduction of water vapor into the cavity affect its development and evolution?
4. High-fidelity measurements of projectile acceleration, projectile surface stresses, contact line position, and cavity pressure using projectile-mounted sensors need to be acquired.

DISCLOSURE STATEMENT

The authors are not aware of any biases that might be perceived as affecting the objectivity of this review.

ACKNOWLEDGMENTS

We would like to thank the ONR ULI (University Laboratory Initiative), grant N00014-06-1-0445 by Theresa McMullen (ONR code 333), for providing thesis support for T.T.T. and the ULI, grant N000141110872 from Maria Medeiros. We are grateful to the Naval Research Enterprise Internship Program (NREIP) and Dr. David Beal, Dr. Jason Gomez, Dr. Robert Kuklinski, and Joseph Miranda at the Naval Undersea Warfare Center (NUWC) for the opportunity to work for several summers on this research in Rhode Island. We acknowledge the Massachusetts Institute of Technology and the Department of Mechanical and Ocean Engineering at MIT as well as Alexandra Techet for their support both in and outside the laboratory. We also thank the Brigham Young University Department of Mechanical Engineering and the Thayer School of Engineering at Dartmouth College for providing high-speed cameras, space, and support. Finally, J.B. thanks the NUWC In-house Laboratory Independent Research (ILIR) for funding support (monitored by Drs. Tony Ruffa and Neil Dubois).

LITERATURE CITED

Abelson HI. 1970. Pressure measurements in the water-entry cavity. *J. Fluid Mech.* 44:129–44

Abelson HI. 1971. A prediction of water-entry cavity shapes. *Trans. ASME D* 93:501–4

Antkowiak A, Bremond N, Le Dizès S, Villermaux E. 2007. Short-term dynamics of a density interface following an impact. *J. Fluid Mech.* 577:241–50

Aristoff J, Bush J. 2009. Water entry of small hydrophobic spheres. *J. Fluid Mech.* 619:45–78

Aristoff JM, Truscott TT, Techet AH, Bush JWM. 2008. The water-entry cavity formed by low Bond number impacts. *Phys. Fluids* 20:091111

Aristoff JM, Truscott TT, Techet AH, Bush JWM. 2010. The water entry of decelerating spheres. *Phys. Fluids* 22:032102

Ashley S. 2001. Warp drive underwater. *Sci. Am.* 284:70–79

Belden J, Jandron MA, Truscott TT. 2013. Physics of elastic spheres skipping on water. In *On the Physics of Sports*, ed. C Clanet. Paris: Ed. l'Ecole Polytech.

Bell GE. 1924. On the impact of a solid sphere with a fluid surface. *Philos. Mag.* 48:753–64

Bergmann R, van der Meer D, Gekle S, van der Bos A, Lohse D. 2009. Controlled impact of a disk on a water surface: cavity dynamics. *J. Fluid Mech.* 381–409

Birkhoff G, Isaacs R. 1951. *Transient cavities in air-water entry*. Nav. Ordnance Rep. 1490, White Oak, MD

Birkhoff G, Zarantonello EH. 1957. *Jets, Wakes, and Cavities*. Appl. Math. Mech. New York: Academic. 353 pp.

Bodily KG. 2013. *The water entry of slender axisymmetric bodies: forces, trajectories and acoustics*. MS thesis. Brigham Young Univ., Provo, UT

Cheny J, Walters K. 1996. Extravagant viscoelastic effects in the Worthington jet experiment. *J. Non-Newton. Fluid Mech.* 67:125–35

Clanet C, Hersen F, Bocquet L. 2004. Secrets of successful stone skipping. *Nature* 427:29

Dobrovolskaya Z. 1969. On some problems of similarity flow of fluid with a free surface. *J. Fluid Mech.* 36:805–29

Douglas H. 1855. *A Treatise on Naval Gunnery*. London: Conway Marit. 4th ed.

Duclaux V, Caillé F, Duez C, Ybert C, Bocquet L, Clanet C. 2007. Dynamics of transient cavities. *J. Fluid Mech.* 591:1–19

Duez C, Ybert C, Clanet C, Bocquet L. 2007. Making a splash with water repellency. *Nat. Phys.* 3:180–83

Dupeux G, Goff AL, Quéré D, Clanet C. 2010. The spinning ball spiral. *New J. Phys.* 12:093004

Dussan EB V. 1979. On the spreading of liquids on solid surfaces: static and dynamic contact lines. *Annu. Rev. Fluid Mech.* 11:371–400

Enriquez OR, Peters IR, Gekle S, Schmidt LE, Lohse D, van der Meer D. 2012. Collapse and pinch-off of a non-axisymmetric impact-created air cavity in water. *J. Fluid Mech.* 701:40–58

Epps BP. 2010. *An impulse framework for hydrodynamic force analysis: fish propulsion, water entry of spheres, and marine propellers*. PhD thesis. Mass. Inst. Technol., Cambridge, MA

Ern P, Risso F, Fabre D, Magnaudet J. 2012. Wake-induced oscillatory paths of bodies freely rising or falling in fluids. *Annu. Rev. Fluid Mech.* 44:97–121

Faltinsen OM, Zhao R. 1997. Water entry of ship sections and axisymmetric bodies. *Proc. AGARD R-827 FDP Ukr. Inst. Hydromech. Workshop High-Speed Body Motion Water*, ed. B Cantwell, Art. 24–1. Neuilly sur Seine, Fr.: AGARD

Franc JP, Michel JM. 2004. *Fundamentals of Cavitation*. New York: Springer

Gaudet S. 1998. Numerical simulation of circular disks entering the free surface of a fluid. *Phys. Fluids* 10:2489–99

Gekle S, Peters IR, Gordillo JM, van der Meer D, Lohse D. 2010. Supersonic air flow due to solid-liquid impact. *Phys. Rev. Lett.* 104:024501

Gilbarg D, Anderson RA. 1948. Influence of atmospheric pressure on the phenomena accompanying the entry of spheres into water. *J. Appl. Phys.* 19:127–39

Glasheen JW, McMahon TA. 1996. Vertical water entry of disks at low Froude numbers. *Phys. Fluids* 8:2078–83

Gomez JT, Shukla A. 2001. Multiple impact penetration of semi-infinite concrete. *Int. J. Impact Eng.* 25:965–79

Grady RJ. 1979. *Hydroballistics Design Handbook*, Vol. 1. Washington, DC: Nav. Sea Syst. Command Hydromech. Comm.

Grumstrup T, Keller JB, Belmonte A. 2007. Cavity ripples observed during the impact of solid objects into liquids. *Phys. Rev. Lett.* 99:114502

Hassan SE. 1999. *Analysis of hydrodynamic planing forces associated with cavity-riding vehicles*. Tech. Memo. 990085, Nav. Undersea Warf. Cent., Newport, RI

Horowitz M, Williamson CHK. 2010. The effect of Reynolds number on the dynamics and wakes of freely rising and falling spheres. *J. Fluid Mech.* 651:251–94

Hrubes JD. 2001. High-speed imaging of supercavitating underwater projectiles. *Exp. Fluids* 30:57–64

Johnson W. 1998. The ricochet of spinning and non-spinning projectiles, mainly from water. Part II: an outline of the theory and warlike applications. *Int. J. Impact Eng.* 21:25–34

Johnson W, Reid SR. 1975. Ricochet of spheres off water. *J. Mech. Eng. Sci.* 17:71–81

Knapp R, Daily J, Hammitt F. 1970. *Cavitation*. New York: McGraw-Hill

Kocheadorfer P. 1993. *Low cost free flight development testing of a rocket propelled high speed underwater missile*. Final Rep. 02841-5047, Nav. Undersea Warf. Cent., Newport, RI

Korobkin AA, Pukhnachov VV. 1988. Initial stage of water impact. *Annu. Rev. Fluid Mech.* 20:159–85

Korobkin AA, Scolan YM. 2006. Three-dimensional theory of water impact. Part 2. Linearized Wagner problem. *J. Fluid Mech.* 549:343–73

Laverty SM. 2004. *Experimental hydrodynamics of spherical projectiles impacting on a free surface using high speed imaging techniques*. Master's thesis. Mass. Inst. Technol., Cambridge, MA

Lee M, Longoria RG, Wilson DE. 1997. Cavity dynamics in high-speed water entry. *Phys. Fluids* 9:540–50

Logvinovich GV. 1972. *Hydrodynamics of Free-Boundary Flows*. NASA TT F-658. Jerusalem/Springfield, VA: Israel Prog. Sci. Transl. US Dep. Commerce, Natl. Tech. Inf. Serv.

Longuet-Higgins MS, Cokelet ED. 1976. The deformation of steep surface waves on water. I. A numerical method of computation.*Proc. R. Soc. Lond. A* 350:1–26

May A. 1951. Effect of surface condition of a sphere on its water-entry cavity. *J. Appl. Phys.* 22:1219–22

May A. 1952. Vertical entry of missiles into water. *J. Appl. Phys.* 23:1362–72

May A. 1975. *Water entry and the cavity-running behavior of missiles*. Tech. Rep. 20910, Nav. Surf. Weapons Cent., White Oak Lab., MD

May A, Hoover WR. 1963. *A study of the water-entry cavity*. Unclassif. NOLTR 63-264, US Nav. Ordnance Lab., White Oak, MD

May A, Woodhull JC. 1948. Drag coefficients of steel spheres entering water vertically. *J. Appl. Phys.* 19:1109–21

May A, Woodhull JC. 1950. The virtual mass of a sphere entering water vertically. *J. Appl. Phys.* 21:1285–89

Miloh T. 1991. On the initial-stage slamming of a rigid sphere in a vertical water entry. *Appl. Ocean Res.* 13:43–48

Miloh T, Shukron Y. 1991. Ricochet off water of spherical projectiles. *J. Ship Res.* 35:91–100

Moghisi M, Squire PT. 1981. An experimental investigation of the initial force of impact on a sphere striking a liquid surface. *J. Fluid Mech.* 108:133–46

Neaves MD, Edwards JR. 2006. All-speed time-accurate underwater projectile calculations using a preconditioning algorithm. *J. Fluids Eng.* 128:284–96

Ogawa A, Utsuno K, Mutou M, Kouzen S, Shimotake Y, Satou Y. 2006. Morphological study of cavity and Worthington jet formations for Newtonian and non-Newtonian liquids. *Part. Sci. Technol.* 24:181–225

Paryshev EV. 2006. Approximate mathematical models in high-speed hydrodynamics. *J. Eng. Math.* 55:41–64

Plesset MS, Prosperetti A. 1977. Bubble dynamics and cavitation. *Annu. Rev. Fluid Mech.* 9:145–85

Richardson EG. 1948. The impact of a solid on a liquid surface. *Proc. Phys. Soc.* 4:352–67

Rood EP. 1991. Review: mechanisms of cavitation inception. *J. Fluids Eng.* 113:163–75

Rosellini L, Hersen F, Clanet C, Bocquet L. 2005. Skipping stones. *J. Fluid Mech.* 543:137–46

Savchenko Y. 2001. *Supercavitation: problems and perspectives*. Presented at CAV 2001, Int. Symp. Cavitation, 4th, Pasadena, CA

Savchenko Y, Semenenko V, Putilin S, Savchenko V, Naumova Y. 2000. *Theory of stable model motion with ventilated and unventilated supercavities*. Rep., Dep. Free Bound. Flows, Natl. Acad. Sci. Ukr. Inst. Hydromech., Kyiv

Seddon C, Moatamedi M. 2006. Review of water entry with applications to aerospace structures. *Int. J. Impact Eng.* 32:1045–67

Shi HH, Itoh M, Takami T. 2000. Optical observation of the supercavitation induced by high-speed water entry. *J. Fluids Eng.* 122:806–10

Shin J, McMahon TA. 1990. The tuning of a splash. *Phys. Fluids* 2:1312–17

Snoeijer JH, Andreotti B. 2013. Moving contact lines: scales, regimes, and dynamical transitions. *Annu. Rev. Fluid Mech.* 45:269–92

Techet A, Truscott T. 2011. Water entry of spinning hydrophobic and hydrophilic spheres. *J. Fluids Struct.* 27:716–26

Thoroddsen ST, Etoh TG, Takehara K, Takano Y. 2004. Impact jetting by a solid sphere. *J. Fluid Mech.* 499:139–48

Truscott TT. 2009. *Cavity dynamics of water entry for spheres and ballistic projectiles*. PhD diss. Mass. Inst. Technol., Cambridge, MA

Truscott TT, Beal DN, Techet AH. 2009. Shallow angle water entry of ballistic projectiles. *Proc. Cav2009 Int. Symp. Cavitation*, ed. S Ceccio, Art. 100

Truscott TT, Epps BP, Techet AH. 2012a. Unsteady forces on spheres during free-surface water entry. *J. Fluid Mech.* 704:173–210

Truscott TT, Techet AH. 2009a. A spin on cavity formation during water entry of hydrophobic and hydrophilic spheres. *Phys. Fluids* 21:121703

Truscott TT, Techet AH. 2009b. Water entry of spinning spheres. *J. Fluid Mech.* 625:135–65

Truscott TT, Wright MM, Langley KR, Belden J. 2012b. Holy balls! Balls that walk on water. *Phys. Fluids* 24:091103

Vakarelski IU, Marston JO, Chan DYC, Thoroddsen ST. 2011. Drag reduction by Leidenfrost vapor layers. *Phys. Rev. Lett.* 106:214501

von Kármán T. 1929. *The impact on seaplane floats during landing*. Tech. Note 321, Natl. Advis. Comm. Aeronaut., Washington, DC

Wagner H. 1932. Phenomena associated with impacts and sliding on liquid surfaces. *ZAMM* 12:193–235

Weiland C, Vlachos PP. 2012. Time-scale for critical growth of partial and supercavitation development over impulsively translating projectiles. *Int. J. Multiphase Flow* 38:73–86

Worthington AM, Cole RS. 1897. Impact with a liquid surface, studied by the aid of instantaneous photography. *Philos. Trans. R. Soc. Lond. A* 189:137–48

Yan H, Liu Y, Kominiarczuk J, Yue DKP. 2009. Cavity dynamics in water entry at low Froude numbers. *J. Fluid Mech.* 641:441–61

Zhao R, Faltinsen O. 1993. Water entry of two-dimensional bodies. *J. Fluid Mech.* 246:593–612